Roger Creel
Machine Learning Final project
December 2019

Estimating the Amount of Readvance of the West Antarctic Ice Sheet using mid-Holocene European sea level records

Motivation

Antarctica is melting. Conservative estimates forecast that by 2100 the Antarctic Ice Sheet will shed one hundred twenty trillion tons of ice, increasing global sea level by 30 centimeters and flooding more than four million homes in the US alone (Bamber et al., 2019). Physical models that predict future sea level rely on estimates of how relative sea level (RSL) varied during past warm periods. The Holocene Epoch (11,000 years ago – present), which is the current interglacial, represents a prime target for this approach because of its highly resolved RSL records. Despite the abundance of Holocene RSL records relative to older periods, they are still sparse, noisy, and unevenly distributed, with fewer data points south of the equator. Furthermore, until recently no unified Holocene RSL database had been compiled. These limitations have made it difficult to detect Holocene sea level changes detailed enough to verify simulations of future climate.

Reconstructing Holocene RSL therefore requires building statistical models that reduce noise, reliably fill in gaps in space and time, and integrate disparate data into a common framework. The best of these employ a Bayesian statistical framework called Gaussian process regression, which works well on small datasets, provides uncertainty measurements on predictions, and uses prior knowledge about the spatiotemporal covariation of sea level to reduce uncertainties and smooth between measurements. Gaussian process (GP) regression has been successfully used to model sea level regionally on Holocene time scales (Khan et al., 2017). However, global implementation of the technique has been hampered by two factors:

computational expense, and the lack of a comprehensive database of Holocene sea level measurements.

Recent advances make both of these hurdles surmountable. First, the 2015 release of Tensorflow, an open-source Python library optimized for parallelization on graphical processing units, makes Gaussian process regression possible on large datasets. Additionally, Dr. Nicole Khan (University of Hong Kong), has given me access to a Holocene RSL database containing more than 13,000 high--quality entries (Khan et al., 2019) (Figure 1). This database will make it possible to infer spatial patterns and rates of RSL change at unprecedented resolution.

These patterns include solid earth mechanisms that could slow ice sheet melt. Such a negative feedback loop is thought to have stabilized the West Antarctic Ice Sheet (WAIS) in the Holocene. Recent Antarctic field and modeling evidence suggests that during the Holocene some sectors of the WAIS retreated several hundred kilometers further inland than their current positions before glacial isostatic adjustment (GIA, the solid earth response to changes in ice and water loading (Farrell and Clark, 1978)) arrested their retreat and caused them to readvance (Kingslake et al., 2018). Documenting WAIS readvance would place critical constraints on ice sheet stability and improve our understanding of how Antarctica will respond to warming in the next century.

Objectives

For my Machine Learning final project, I construct a Bayesian statistical model that smooths between RSL datapoints in space and time with uncertainties quantified, and can identify different drivers of Holocene RSL. I validate the model's accuracy in differentiating between sea level by applying the model to a simplified, synthetic Holocene RSL dataset. I have

constructed a variety of GIA simulations based on an ensemble of different mantle viscosity profiles, lithospheric thicknesses, and deglacial ice reconstructions, which are the key parameters in GIA models. I have also modeled a sea-level pattern of WAIS retreat and readvance, to which I have applied uncertainties based on recent field evidence from Antarctica (Kingslake et al., 2018) (fig. 2). I add these spatiotemporal patterns together to create a realistic Holocene RSL scenario whose magnitude reflects the varying sea-level contributions from GIA and readvance sources.

To produce the synthetic "true" sea-level field, I sample the scenarios at the location and time of each real datapoint. I then interpolate between points using GP regression to generate a best-fit RSL estimate, and decompose this estimate into distinct temporal and spatial patterns. I then compare these patterns to the original inputs of the synthetic scenario. A match allows the identification of the same patterns in the real Holocene database. A failure to match suggests that the original RSL input is too small to be detected.

This synthetic model allows me to estimate the minimum magnitude of West Antarctic Ice Sheet readvance detectable with mid-Holocene European sea level records (fig. 3). Using a suite of GIA models as prior knowledge, I then incorporate the real sea-level database into a continuous model of European sea level during the mid-Holocene. Finally, I use the differences between GIA models and the real RSL data as a tool to understand the complex processes that contributed to Holocene sea level fluctuations.

Data

My dataset is composed of 1017 sea level indicator points (SLIP) from European coastal areas, all radiocarbon dated to be between 3000 and 7000 years old (fig. 4). Europe is useful as a

test case because it contains a large number of RSL datapoints in a small geographic area. These data come from a variety of sources depending on location. In the British Isles, the data derive principally from salt marshes and isolation basins. Salt marshes ecosystems grow continuously at sea level, their upper marshes flooded only at astronomical high tide, their lower marshes constantly flooded even at neap tide. By coring these systems and dating foraminifera at the freshwater-brackish-marine transition, it is possible to calculate an indicative range for the SLIP, i.e. the relationship of the SLIP to ancient sea level (Shennan et al., 2018). The uncertainties in salt marsh records typically depend on tidal range magnitude. Tidal ranges for the mid-late Holocene are typically assumed to be similar to present-day ranges, though that assumption loses validity for early Holocene samples (e.g. Hill et al., 2016).

At northern European sites near the locations of the Last Glacial Maximum ice sheets, isostatic rebound has uplifted glacially-carved marine fjords such that they became cut off from the ocean. These "isolation basins," now lakes, record the marine to freshwater transition, which serves as a SLIP with typical standard deviation $\pm$ 1 meter. At other near-field sites, GIA uplifted boulder beaches. Organisms trapped under rocks on those beaches can serve as terrestrial- or marine-limiting SLIPs. In places where Neolithic humans lived, charcoal or human remains can also indicate a terrestrial bounding SLIP.

Mediterranean sea-level data come from a more diverse set of indicators. A majority of Mediterranean SLIPs come from sedimentary archives such as lagoons. Like salt marshes at high latitudes, Mediterranean lagoons retain continuous records of the elevation at which sea water transitioned through brackish to fresh water. Radiocarbon dates of foraminifera living at this transition, along with estimates of tidal range at that location, provide an indicative range for each SLIP. Similar calculations are possible on preserved specimens of *Posidonia oceanica*, the

ubiquitous Mediterranean sea grass that grows near sea level. Archeological sites also provide useful sea-level reference points. The elevations of Roman quarries, fish ponds, and wells, for instance, place tight bounds on local relative sea level, as do Neolithic burial sites. Uncertainty estimates for these SLIPs vary from ~ $\pm$ 0.3 meters (wells) to $\pm$ > 5 meters (undifferentiated salt marsh).

Methodology

To account for the sparseness, scarcity, and uneven distribution of Holocene RSL data, the sea level change modeling community has adopted a variety of statistical techniques (Kopp et al., 2009; Kopp et al. 2016). Some of these techniques are simple. For example, over millennial time scales at single locations, simple linear regression through the midpoints of sea level indicator points, ignoring temporal or vertical uncertainties, can reasonably approximate sea level trends (e.g. Shennan et al., 2002; Engelhart et al., 2012). For longer time scales, a 'change-point' model is sometimes adopted, which represents sea level as a series of separate, linear, continuous sections and is typically used to estimate changes in RSL rates (e.g. Kemp et al., 2015; Long et al. 2014). These models assume that the processes underlying the sea level change are linear.

Gaussian process (GP) regression, also known as kriging, least squares collocation, or generalized least squares interpolation, offers a more statistically robust methodology for interpolating between noisy, sparse measurements (Rasmussen and Williams, 2006). GP regression does not assume that the processes underlying data, i.e. the latent processes, can be parameterized via a single function or set of functions. Instead, it is assumed only that the latent processes can be characterized by classes of covariance functions, or "kernels".

The characteristics of these covariance functions are determined by hyperparameters such as length-scale, smoothness, and functional form. Length-scale of covariance describes the distance beyond which two points in n-dimensional space cease to appreciably covary. Smoothness is synonymous with differentiability. Examples of functional forms include linear, constant, and periodic. Initial hyperparameters in GP regression are chosen to represent *a priori* knowledge about latent processes. For instance, the spatial length-scale of GIA covariation is known to be between 500 and 5000 km, and its temporal length-scale between 5000 and 20000 years.

Covariance kernels specify a joint multivariate normal probability distribution for any finite set of variables. These variables together are completely described by their mean and normally distributed covariance kernel, which can be composed of the combination of one or many covariance matrixes, each specifying a latent process. When combined with a likelihood function governed by the difference between measured and predicted data and weighted by the uncertainty covariances of individual measured data points, the product is a posterior probability density function that quantifies the likelihood of the predicted given measured data and prior-specified covariance kernels (Rasmussen and Williams, 2006). The hyperparameters of the GP regression are then tuned via gradient descent optimization to minimize the negative log likelihood of the model given the data and their uncertainties.

I perform GP regression on two versions of the European Holocene RSL database. As outlined above, I first regress a simplified version of the database composed of GIA and readvance signals. I then conduct GP regression on the 1017 datapoints in the real European Holocene RSL database. To capture the known spatial and temporal variability of Holocene RSL, I use one spatial and two temporal kernels, each of them having the once-differentiable Matern 3/2 form. The optimized length-scale hyperparameter for the spatial kernel is calculated

in degrees latitude/longitude. The temporal kernels are calculated in years. The algorithm is written using GPflow, a TensorFlow-based python library (Matthews et al., 2016). Gradient descent optimization is performed with the Scipy python library.

Results

At all locations, spatiotemporal GP regression improves the prior estimate of RSL and decreases uncertainties (fig. 5). At every site where "true" data fall within prior uncertainty estimates, posterior RSL estimates pass through data with uncertainties. In areas with sparse or highly uncertain data (e.g. Normandy), the spatiotemporal proximity of other data still diminish uncertainties. Where "true" data fall outside the prior 95% confidence interval, the posterior RSL estimate falls as close as possible to both "true" data and prior. GIA prior uncertainty estimates increase near ice sheets because of greater near-field sea-level sensitivity to GIA model parameters. Spatial and temporal uncertainties are reduced in a radius around each datapoint that corresponds to the optimized hyperparameter length-scale. The long length-scale of temporal sea-level covariance therefore keeps uncertainties low near any location with even a single sea-level datapoint in space-time.

The learned difference between "true" data and prior field is largest near areas covered during the Last Glacial Maximum by the Scottish Ice Sheet (fig. 6). This makes sense because "true" sea level was generated with a mantle viscosity parameterization that caused post-LGM solid earth rebound faster than the prior mean scenario. The GP regression learns no information about the sea-level drawdown near the former Fennoscandian ice sheet. It should not be expected to, as no sea-level data exist in this dataset. However, sea level near the Fennoscandian ice sheet would be expected to fall during the Holocene because of the ongoing effects of GIA.

In this case, then, information known *a priori* improves the best guess of sea level beyond data constraints. This relationship works best in data-rich areas. Where no data exist, the model reverts to the prior. Model prediction in data-sparse locations therefore is strongly controlled by choice of prior and worsens with distance from datapoints according to the optimized lengthscale of kernel covariance.

Initially, I used four covariance functions: spatial and temporal kernels for GIA, and spatial and temporal kernels for WAIS readvance. The small magnitude and long spatial length-scale of WAIS readvance, however, means that its spatial distribution across Europe is not distinguishable from the more complex spatial pattern of GIA. A second spatial kernel therefore does not appreciably impact the likelihood of the results, so I simplified the model to one spatial and two temporal kernels (GIA + readvance).

Because the composite posterior covariance function is the additive combination of functions with distinct hyperparameters, it can be decomposed into individual components. Comparing the prior readvance signal and the posterior makes it possible to determine whether the readvance was large enough to be detectable by the GP regression. A realistic readvance, equivalent to a maximum far-field magnitude of 0.6 meters RSL fall, cannot be detected with only European RSL records 7–3 ka: the decomposed posterior is indistinguishable from the prior. As the readvance signal is increased, however, the uncertainties on its corresponding decomposed GP kernel shrink. When the magnitude of reavance passes 1.2 meters RSL equivalent, it becomes detectable (fig. 7). Scaled even further, to 3.0 meters, it becomes virtually certain to have occurred within uncertainties.

A GIA prior also improves GP regression on real sea level data (fig. 8). The difference between real data and GP regression reveals systematic patterns in the misfit between GIA model

mean and RSL data. As occurred in the synthetic case, the GIA model mean overpredicts RSL near the area covered by the Scottish Ice Sheet. This overprediction is apparent in the learned difference between data and model. However, unlike in the synthetic case, the model also overpredicts sea level in all of the Mediterranean and along the western margin of the Atlantic, save for RSL near the Bay of Biscay, where RSL is underpredicted. Conversely, the GIA model mean consistently underpredicts sea level around England.

The similarity between the synthetic data-model misfit and the real data-model misfit around Scotland suggests that the GIA model with 71 km lithosphere, upper mantle viscosity of 2e20 Pa s, and lower mantle viscosity of 5e21 Pa s, better approximates real Holocene RSL than a GIA model with 71 km lithosphere and a suite of mantle viscosities that span the space of realistic possibility. However, the sharp gradient in RSL misfit across the British Isles indicates persistent data-model misfits that cannot be explained solely by the choice of radial mantle viscosity GIA model.

A number of effects contribute to the difference between GIA models and the real RSL data. Relative sea level near ice sheets is particularly sensitive to variations in mantle viscosity and lithospheric thickness (Hay et al., 2016). The solid earth structure beneath both the British Isles and Scandinavia is thought to be highly heterogenous (Baykiev et al. 2018; Barnhoorn et al. 2011). Previous research on Mediterranean sea level indicators suggests that heterogenous mantle composition may also influence Mediterranean sea level during the Holocene (Vacchi et al., 2018). Such heterogeneity would effect the longterm GIA response to deglaciation.

Additionally, GIA models depend on ice sheet histories, which are also uncertain. ICE-6G, the single deglacial ice sheet history used in these GIA models, is calibrated with a number of bounds including present-day measurements of vertical crustal motion and gravity anomalies

(Peltier et al., 2015). It does not, however, include data from moraines and other terrestrial proxy data, nor does it have internally consistent ice mechanics (Purcell et al., 2016). A global deglacial ice history that included these bounds, similar to the Laurentide ice history constructed by Tarasov and others (2012), would better approximate the cryospheric distribution and thickness since the Last Glacial Maximum.

As mentioned above, other effects beyond GIA also contributed to Holocene RSL changes. Norwegian relative sea level data include the so-called "Tapes Transgression," a local sea-level transgression in the mid-Holocene which current GIA models do not reproduce (e.g. Svendsen et al., 1987). The Tapes Transgression is not visible in sea level records outside of Northern Europe. Changes in ocean circulation patterns, possibly connected to the draining of proglacial lake Agassiz at ~8.2 ka, may explain this transgression. Retreat and readvance of the Greenland Ice Sheet during the mid-Holocene, though of much smaller magnitude than the putative WAIS readvance (Lecavalier et al. 2014), may also contribute to the patterns recorded by the real RSL data.

Bibliography

Bamber, J. L., Riva, R. E. M., Vermeersen, B. L. A. & LeBrocq, A. M. Reassessment of the Potential Sea-Level Rise from a Collapse of the West Antarctic Ice Sheet. *Science* **324**, 901–903 (2019).

Baykiev, E., Guerri, M. & Fullea, J. Integrating Gravity and Surface Elevation With Magnetic Data: Mapping the Curie Temperature Beneath the British Isles and Surrounding Areas. *Front. Earth Sci.* **6**, (2018).

Barnhoorn, A., Wal, W. van der, Vermeersen, B. L. A. & Drury, M. R. Lateral, radial, and temporal variations in upper mantle viscosity and rheology under Scandinavia. *Geochemistry, Geophysics, Geosystems* **12**, (2011).

Engelhart, S.E., Horton, B.P., 2012. Holocene sea level database for the Atlantic coast of the United States. Quat. Sci. Rev. 54, 12e25. https://doi.org/10.1016/j.quascirev.2011.09.013.

Farrell, W. E. & Clark, J. A. On Postglacial Sea Level. *Geophysical Journal of the Royal Astronomical Society* **46**, 647–667 (1976).

Hay, C. C. *et al.* Sea Level Fingerprints in a Region of Complex Earth Structure: The Case of WAIS. *J. Climate* **30**, 1881–1892 (2016).

Hill, D. F. Spatial and Temporal Variability in Tidal Range: Evidence, Causes, and Effects. *Curr Clim Change Rep* **2**, 232–241 (2016).

Kemp, A.C., Horton, B.P., Vane, C.H., Corbett, D.R., Bernhardt, C., Engelhart, S.E., Anisfeld, S.C., Parnell, A.C., Cahill, N., 2013. Sea-level change during the last 2500 years in New Jersey, USA. Quat. Sci. Rev. 81, 90e104.

Khan, N. S. *et al.* Drivers of Holocene sea-level change in the Caribbean. *Quaternary Science Reviews* **155**, 13–36 (2017).

Khan, N. S. *et al.* Inception of a global atlas of sea levels since the Last Glacial Maximum. *Quaternary Science Reviews* **220**, 359–371 (2019).

Kingslake, J. *et al.* Extensive retreat and re-advance of the West Antarctic Ice Sheet during the Holocene. *Nature* **558**, 430 (2018).

Kopp, R. E., Simons, F. J., Mitrovica, J. X., Maloof, A. C. & Oppenheimer, M. Probabilistic assessment of sea level during the last interglacial stage. *Nature* **462**, 863–867 (2009).

Kopp, R. E. *et al.* Temperature-driven global sea-level variability in the Common Era. *PNAS* **113**, E1434–E1441 (2016).

Lecavalier, B. S. *et al.* A model of Greenland ice sheet deglaciation constrained by observations of relative sea level and ice extent. *Quaternary Science Reviews* **102**, 54–84 (2014).

Long, A., Barlow, N., Gehrels, W., Saher, M., Woodworth, P., Scaife, R., Brain, M., Cahill, N., 2014. Contrasting records of sea-level change in the eastern and western North Atlantic during the last 300 years. Earth Planet Sci. Lett. 388, 110e122.

Matthews, A. G. de G. *et al.* GPflow: A Gaussian process library using TensorFlow. *arXiv:1610.08733 [stat]* (2016).

Peltier, W. R., Argus, D. F. & Drummond, R. Space geodesy constrains ice age terminal deglaciation: The global ICE-6G_C (VM5a) model. *Journal of Geophysical Research: Solid Earth* **120**, 450–487 (2015).

Purcell, A., Tregoning, P. & Dehecq, A. An assessment of the ICE6G_C (VM5A) glacial isostatic adjustment model. *Journal of Geophysical Research: Solid Earth* **121**, n/a-n/a (2016).

Rasmussen, C. E. & Williams, C. K. I. *Gaussian processes for machine learning*. (MIT Press, 2006).

Shennan, I., Bradley, S. L. & Edwards, R. Relative sea-level changes and crustal movements in Britain and Ireland since the Last Glacial Maximum. *Quaternary Science Reviews* **188**, 143–159 (2018).

Shennan, I., Peltier, W.R., Drummond, R., Horton, B., 2002. Global to local scale parameters determining relative sea-level changes and the post-glacial isostatic adjustment of Great Britain. Quat. Sci. Rev. 21, 397e408.

Svendsen, J. I. & Mangerud, J. Late Weichselian and holocene sea-level history for a cross-section of western Norway. *Journal of Quaternary Science* **2**, 113–132 (1987).

Tarasov, L., Dyke, A. S., Neal, R. M. & Peltier, W. R. A data-calibrated distribution of deglacial chronologies for the North American ice complex from glaciological modeling. *Earth and Planetary Science Letters* **315–316**, 30–40 (2012).

Vacchi, M., Marriner, N., Christophe, M., Spada, G., Alessandro, F., & Rovere, A. Multiproxy assessment of Holocene relative sea-level changes in the western Mediterranean: Sea-level variability and improvements in the definition of the isostatic signal. *Earth-Science Reviews* **155,** 172-197 (2016)

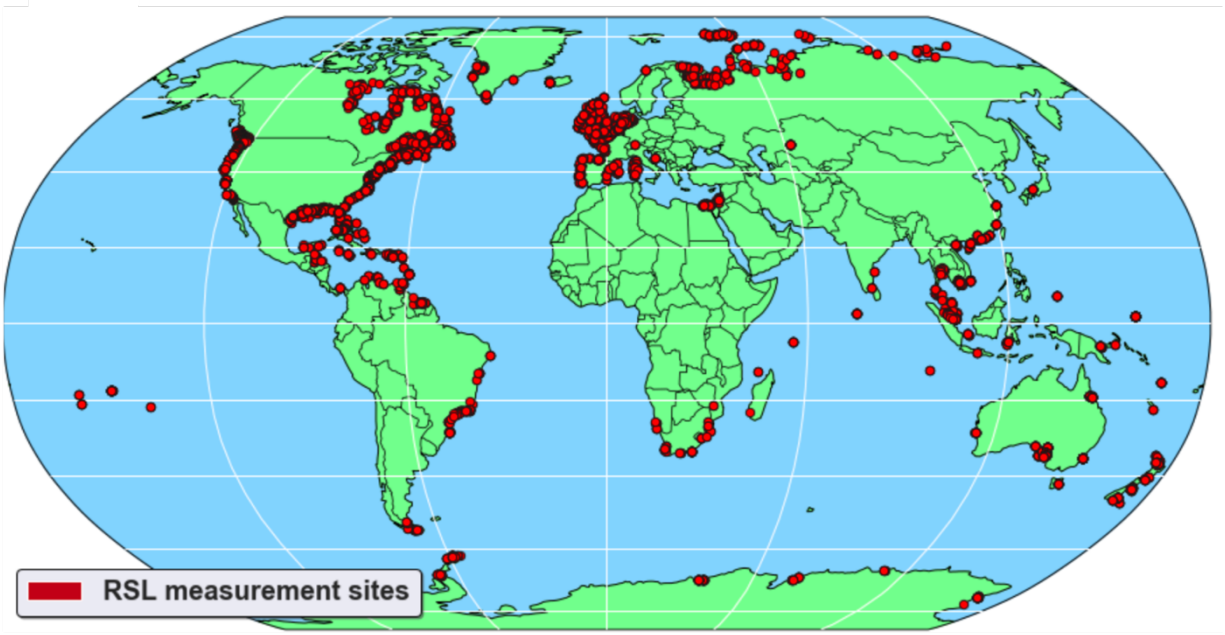

Figure 1. Holocene RSL database, 12 ka to present (Khan et al., 2019). Red dots mark locations of sea level indicator points.

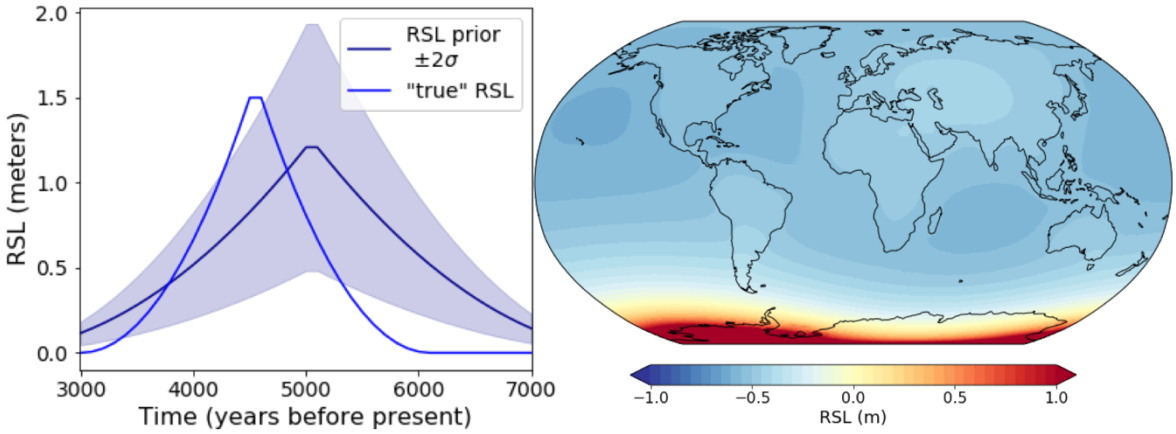

Figure 2. A) Synthetic scenario of readvance in blue; estimate of readvance likelihood based on Kingslake et al (2018) in navy. B) Elastic fingerprint of WAIS readvance. The spatiotemporal patterns of WAIS readvance and GIA determine the covariance functions of a GP regression conditioned on the readvance and GIA priors. The deglacial GIA prior, based on an ICE-6G and a suite of rheological parameters, is not shown here.

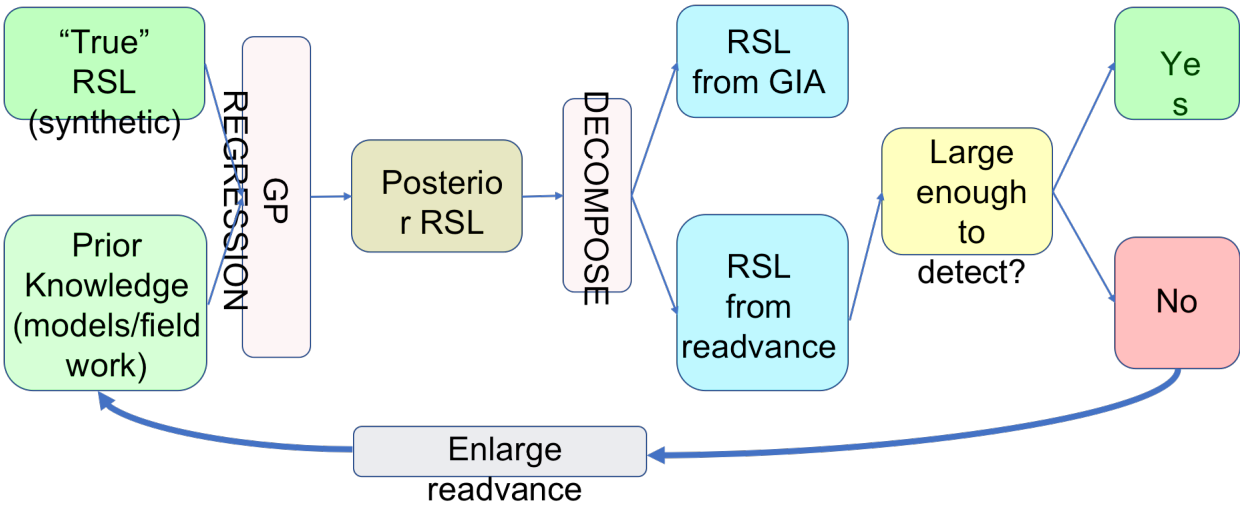

Figure 3. Schematic diagram of workflow for WAIS readvance detection algorithm using Holocene RSL records.

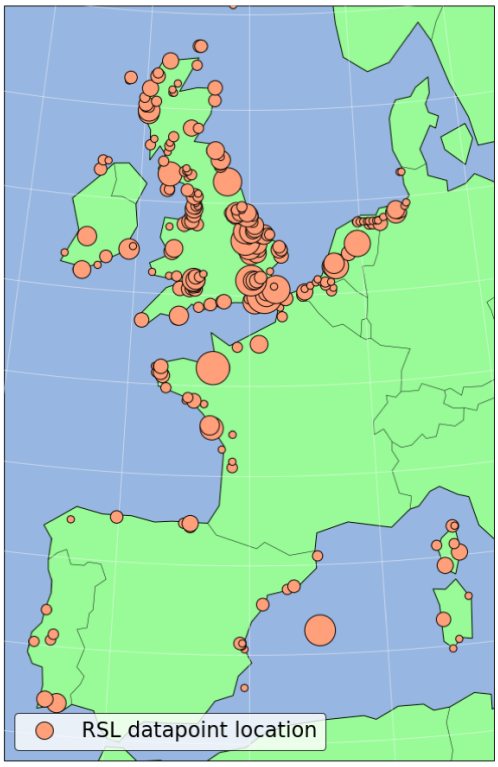

Figure 4. Holocene RSL database, Europe 7-3 ka. Circle sizes scale with number of datapoints.

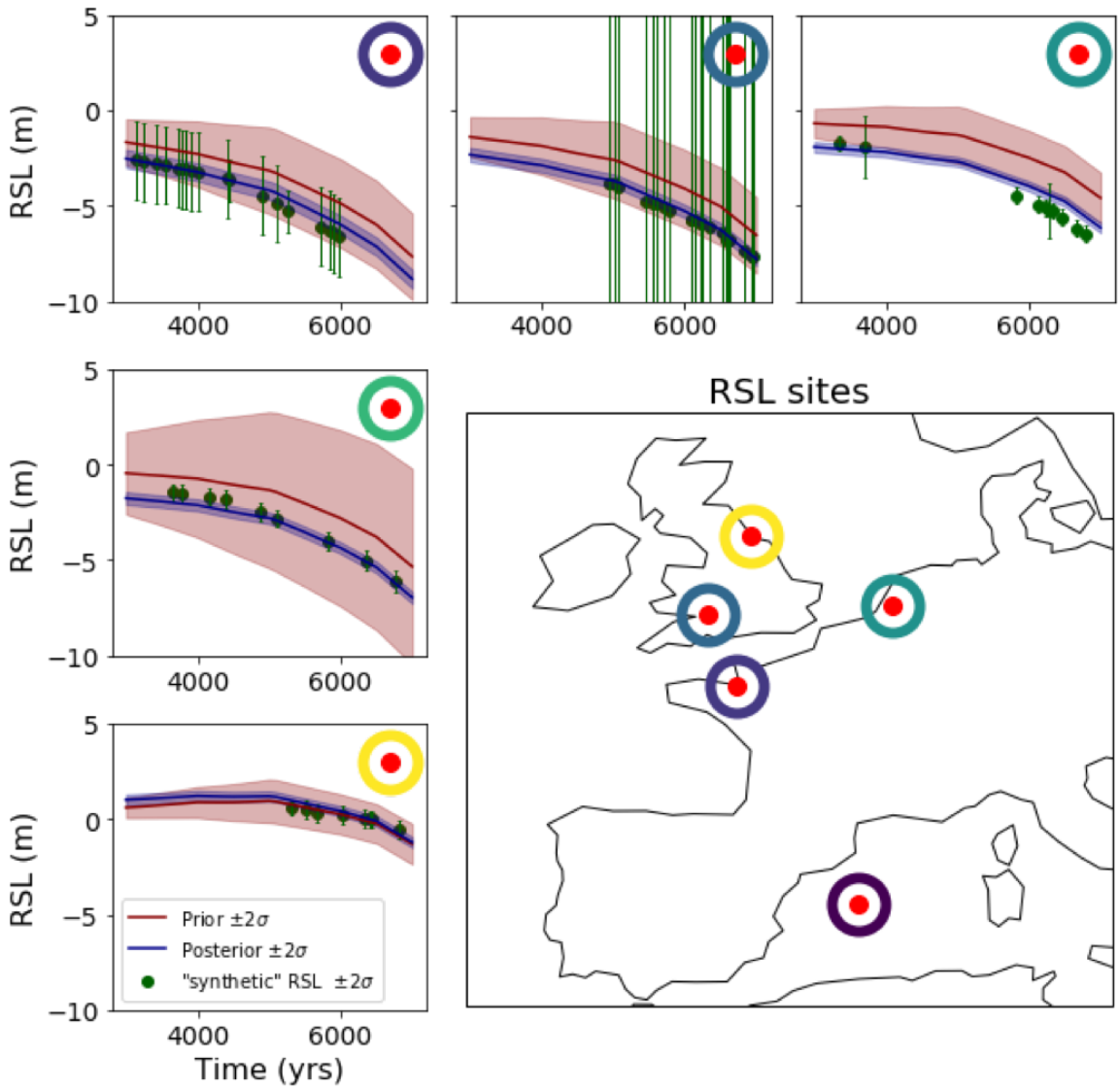

Figure 5. GP Regression on RSL Data 7-3ka. Green dots are “true” RSL data. Red line is GIA + readvance prior. Blue line is posterior.

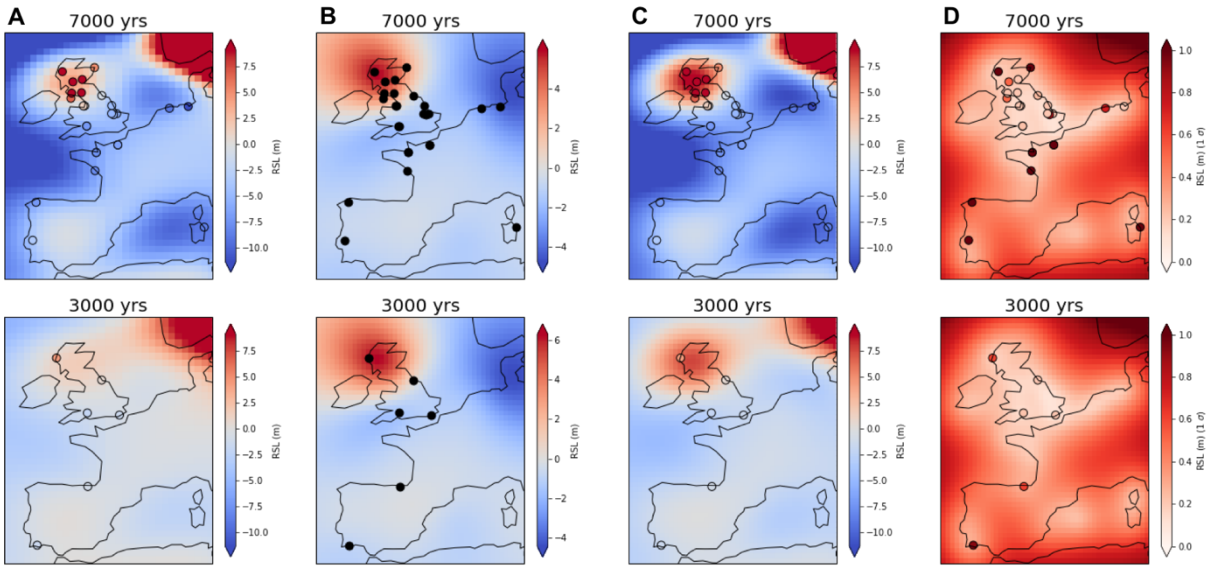

Fig 6. Spatiotemporal GP regression on synthetic European RSL data 7-3ka. A) Circles are synthetic "true" data, field is mean of the RSL prior. B) Learned difference between prior RSL estimate and "true" data. C) Posterior RSL given prior estimate. D) Standard deviation of posterior RSL estimate.

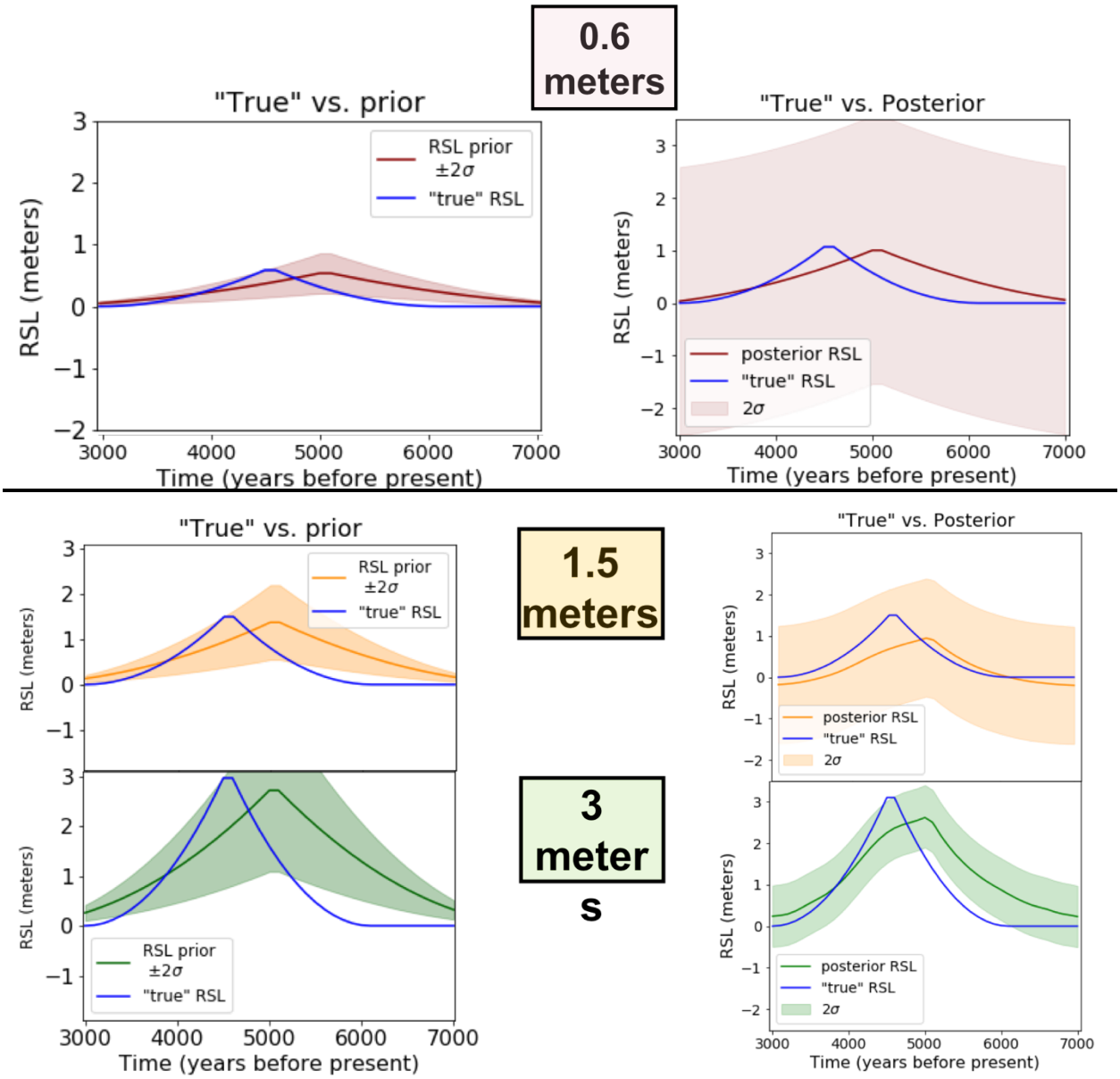

Figure 7. Prior and posterior temporal patterns of WAIS readvance compared to "true" readvance of different magnitudes for the same "true" signal.

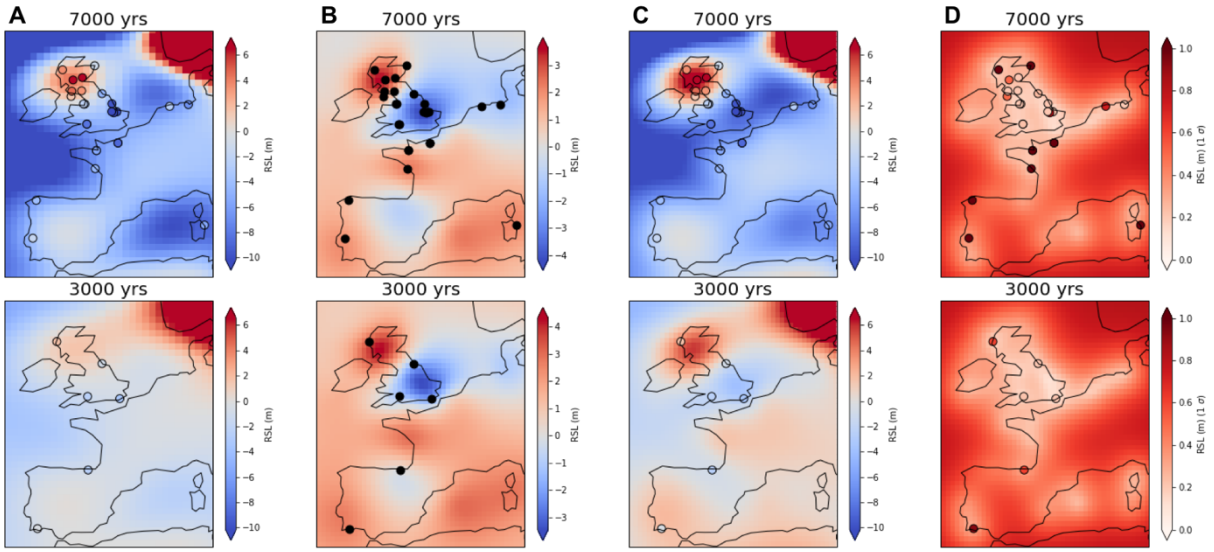

Figure 8. Spatiotemporal GP regression on real European RSL data 7-3ka. A) Circles are RSL data, field is mean of the GIA prior. B) Learned difference between GIA model mean prior and RSL data. C) Posterior RSL given prior estimate. D) Standard deviation of posterior RSL estimate.